Kondo-lattice-mediated interactions in flat band systems

Pramod Kumar,¹ Guangze Chen,¹ and J. L. Lado¹

¹Department of Applied Physics, Aalto University, 00076 Aalto, Espoo, Finland
(Dated: July 12, 2021)

Electronic flat bands represent a paradigmatic platform to realize strongly correlated matter due to their associated divergent density of states. In common instances, including electron-electron interactions leads to magnetic instabilities for repulsive interactions and superconductivity for attractive interactions. Nevertheless, interactions of Kondo nature in flat band systems have remained relatively unexplored. Here we address the emergence of interacting states mediated by Kondo lattice coupled to a flat band system. Combining dynamical mean-field theory and tensor networks methods to solve flat band Kondo lattice models in one and two dimensions, we show the emergence of a robust underscreened regime leading to a magnetically ordered state in the flat band. Our results put forward flat band Kondo lattice models as a platform to explore the genuine interplay between flat band physics and many-body Kondo screening.

I. INTRODUCTION

Flat band systems represent one of the paradigmatic systems to engineer correlated matter [1–6]. Quantum engineering has provided a variety of platforms potentially combining both flat bands and interactions, including atomic lattices [7–10], cold atoms [11–13] and twisted moire materials[14–16]. Their potential for correlated physics stems from the vanishing electronic dispersion. which creates a greatly enhanced density of states at the Fermi energy [17–20]. While a wide variety of correlated states in flat band systems can emerge, minimal attractive or repulsive on-site interactions are well known to lead to magnetism and superconductivity, respectively [2, 21–27]. More complex interactions in flat bands are also well known to give rise to other symmetry broken states, including charge density waves and bond orders [28-31]. The different interactions considered are usually written as an effective density-density interaction. Nevertheless, external couplings such as Kondo couplings [32, 33] in the system can lead to even more sophisticated interaction terms.

Electronic states coupled to magnetic impurities are known as prototypical many-body states [34, 35]. The simplest example corresponds to the Kondo problem, in which a single magnetic impurity forms a many-body ground state with its electronic bath [34–36]. The lattice version of the problem, known as the Kondo-lattice problem, represents the starting point for exotic physical phenomena found in heavy-fermion systems [34, 37– 44]. Interestingly, the Kondo physics outlined above is usually addressed in systems with strong electronic dispersion, while the Kondo problem for flat bands has been much less explored [45–49]. In the dispersive limit, the interaction between a local magnetic impurity and the conduction bath is determined by the Kondo temperature, increasing with the density of states, and therefore divergent in the flat band regime. The coupling between magnetic impurities, known as Ruderman-Kittel-Kasuya-Yosida interaction[50-52], is determined by the Fermi wavelength of the conduction bath.

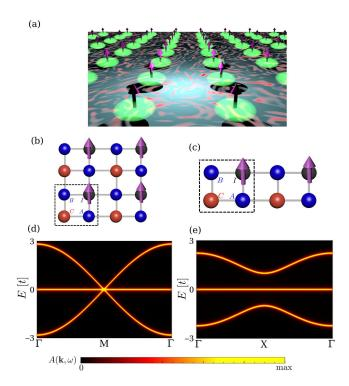


FIG. 1. (a) Sketch of a Kondo lattice coupled to a flat band electron gas. Panels (b, c) show the lattice model realizing a flat band Kondo lattice model in two dimensional (b) and one dimension (c). Panels (d, e) show the momentum resolved spectral function $A(\mathbf{k},\omega)$ of the flat band electron gas of panels (b, c) respectively.

However, in the flat band limit, the previous picture breaks down due to the absence of a well defined Fermi surface.

Here we address the fate of a flat band system coupled to a lattice of magnetic impurities, realizing the so-called flat band Kondo lattice model. We observe that the system develops a robust local magnetic order, overcoming Kondo screening effects of the flat band. We demonstrate that the full phenomenology can be captured by symmetry broken mean-field method, and compare these results with two genuine many-body methods, dynamical mean-field theory and tensor networks states. Our results demonstrate the non-trivial impact of flat bands in Kondo lattice problems, emphasizing the complex interplay between exchange and Kondo physics in flat band systems.

The manuscript is organized as follows. In section II, we introduce the minimal models featuring a flat-band Kondo lattice physics, both in one dimension and two-dimensions. In section III we present the solution of the two-dimensional flat band Kondo lattice model as solved by dynamical mean field theory. In section IV we present the solution of the one-dimensional flat band Kondo lattice model as solved with tensor networks. Finally, in section V we summarize our conclusions.

II. FLAT BAND KONDO LATTICE MODEL

In the following we describe the effective models used to capture a flat band Kondo lattice model, as shown in Fig. 1 (bc). The full Hamiltonian $\mathcal{H} = \mathcal{H}_0 + \mathcal{H}_{\rm int}$ has both non-interacting \mathcal{H}_0 and interacting $\mathcal{H}_{\rm int}$ terms. Let us start with the non-interacting term, for which we take a first neighbor spinful model of the form

$$\mathcal{H}_0 = t \sum_{\langle ij \rangle, \sigma} c_{i\sigma}^{\dagger} c_{j\sigma} \tag{1}$$

where $c_{i\sigma}$ is the annihilation operator for site i and spin σ , and $\langle \rangle$ denotes nearest-neighbor sites. The lattices considered for Eq. 1 would be a square lattice and a ladder, for the two-dimensional and one-dimensional cases, respectively. In both cases, the fundamental unit cell of the system consists of four spinful sites.

Let us now address the interacting term of the Hamiltonian. In each unit cell of the system, we will include interactions solely in a single site, which we label by I in the form

$$\mathcal{H}_{\text{int}} = U \sum_{I} \left(n_{I\uparrow} - \frac{1}{2} \right) \left(n_{I\downarrow} - \frac{1}{2} \right), \tag{2}$$

where $n_{I\sigma}=c_{I\sigma}^{\dagger}c_{I\sigma}$ and U>0 is the interaction strength. The interaction acts only at one of every four sites, namely the sites labelled as I, which in the following will be referred to as the impurity site. It is worth to note that by definition, the previous Hamiltonian leads to a half filled state for arbitrary U. In the strong coupling limit $U\gg t$, the low energy sector realizes a flat band electron gas, as shown in Figs. 1de. The interacting site develops a local magnetic moment, leading to a low energy effective Hamiltonian for the full system of the form

$$\mathcal{H}_{\text{eff}} = t \sum_{\langle ij \rangle', \sigma} c_{i\sigma}^{\dagger} c_{j\sigma} + \sum_{\langle Ij \rangle''} J \mathbf{S}_{\mathbf{I}} \cdot \tau_{\sigma, \sigma'} c_{j, \sigma}^{\dagger} c_{j, \sigma'}$$
(3)

where $\langle ij \rangle'$ denotes the sum over first neighboring non-interacting sites, and $\langle Ij \rangle''$ denotes the sum over first neighbors with I an impurity site and j a non-interacting site. The effective Kondo coupling J depends on the interaction U as $J \sim t^2/U$. In the following we will work with the full fermionic Hamiltonian \mathcal{H} , yet the effective Hamiltonian as shown in Eq. 3 will provide useful insights to rationalize the full many-body solution.

Finally, it is worth to comment on the emergence of the flat band in the previous models. In the infinite U limit, one of the four sites is fully disconnected from the other non-interacting sites. In this limit, the two-dimensional and one dimensional models realize a bipartite lattice with a different number of sublattice sites per unit cell, automatically leading to a flat band.[53–56]. For finite U, the system will thus realize a two-dimensional or one-dimensional electron gas coupled to a lattice of Kondo impurities. In the following, we explore this finite-U coupling limit, first in two dimensions with dynamical mean-field theory and later in one dimension with tensor-networks.

III. DMFT APPROACH OT THE TWO DIMENSIONAL FLAT BAND KONDO LATTICE MODEL

In the following, we will address the fate of the twodimensional Kondo lattice problem. We will consider the mean-field solution as a reference, as to see how quantum fluctuations included in the dynamical mean-field approach renormalize the results. Evaluations of the site selective magnetism have been calculated using the cellular mean-field theory, cellular dynamical mean-field theory with continuous time quantum Monte-Carlo method, and exact diagonalization as the impurity solver [57–59]. Within CDMFT, a lattice problem is mapped to a finite cluster coupled to a non-interacting bath. In our case, the cluster is a four site (2×2) plaquette as shown in Fig. 1 [60–62]. We define the site-dependent absolute magnetization for the cluster as $m_i = \langle n_{i\uparrow} \rangle - \langle n_{i\downarrow} \rangle$, where $\langle n_{i,\sigma} \rangle = G_{i,\sigma\sigma}(\tau \to 0^-)$ is the density of spin- σ particles for a given site of the cluster calculated from the local Green's function. To understand the origin of the site-selective magnetic order; we calculate the effective hybridization [63] between the impurity and the sites near it. We can define the nonlocal effective hybridization order for the given four site clusters as

$$\Delta_{\alpha} = |\sum_{\alpha \neq \beta, \sigma} \langle c_{\alpha \sigma}^{\dagger} c_{\beta \sigma} \rangle| = \sum_{\alpha \neq \beta, \sigma} |G_{i, \sigma \sigma}^{\alpha \beta}(\tau \to 0^{-})| \quad (4)$$

where $\alpha(\beta)$ is the sublattice index. The behavior of effective hybridization is proportional to the non-interacting local density of states at the sublattices of the unit cell [36].

In the following, we present the complete magnetic phase diagram in the presence of a finite two-body interaction U at finite temperature T at half-filling, where the

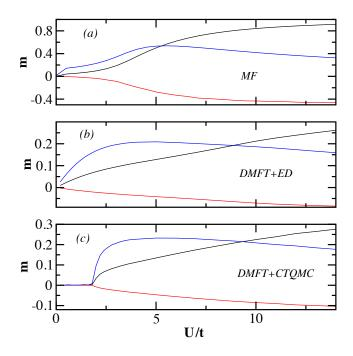


FIG. 2. Magnetic order parameter at impurity site, I (black), at sites next to the impurity, A/B (red), and at the second neighbor site of the impurity site, C (blue), evaluated using (a) mean-field theory [64], (b) dynamical mean-field theory (DMFT) + exact diagonalization (ED), and (c) dynamical mean-field theory (DMFT) + continuous-time quantum Monte-Carlo (CTQMC) for varying interaction strength U. Note that the magnitude of the magnetic order at C site has been scaled by a factor of four for the purpose of visual clarity.

number of particles per site is one. Simultaneously, we also explore the nature of effective Kondo-hybridization on the emergent site-selective magnetization. The role of quantum fluctuations, ignored in the mean field theory, have been addressed by using DMFT.

A. Zero temperature calculations

Due to emergent singularity in the LDOS at different sublattices in the presence of the finite local interaction at the impurity site, the local magnetic order is non-uniform across different sites. We show the spatially resolved magnetic order m_{α} evaluated using Hartree-Fock mean field theory in the Fig. 2(a), zero temperature ED+CDMFT in the Fig. 2(b) and CTQMC+CDMFT at T=0.01 the Fig. 2(c) for varying interaction strength U/t at the impurity site. We allow the breaking of the SU(2) spin-rotation symmetry to capture the magnetically ordered state. An initial self-energy that is constant in the Matsubara frequency is added in this way that it breaks SU(2) symmetry of the Hamiltonian.

For weak to moderate interactions, the local magnetic order at different sublattices gradually develops such that $\operatorname{sign}(m_{A/B}) = -\operatorname{sign}(m_C) = -\operatorname{sign}(m_I)$ for any U/t>0

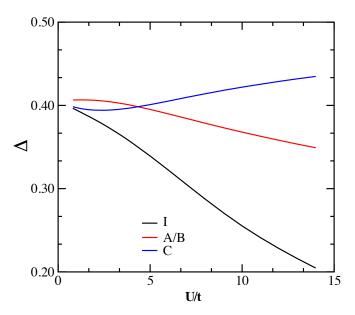


FIG. 3. Effective hybridization of a given sublattice with the rest of the sites in the unit cell as Eq 4.

due to the antiferromagnetic coupling between the local moments at neighboring site of the unit cell. The sizes of the magnetic moments of the A/B, C, and I sites are very different, as expected from the non-uniform nature of the model. While the magnetization of the A/B and I sites saturates with the strength of the interaction, the same does not occur on the site C. Magnetic order at the C site asymptotically goes to zero after attaining the peak at a given U/t. The qualitative behavior obtained from the different approaches is similar for all U/t, however the key aspect is the amplitude of the m_{α} calculated using DMFT is significantly less than to the one obtained from MF approach. This is due to the many-body corrections included in DMFT, not accounted by the mean-field calculations. Interestingly, and despite such differences, it is observed that the flat band electron gas does not fully screen the local moment.

The hybridization between the electrons at non-interacting sites and the impurity site leads to the formation of the singlet between the spins of electrons at different sites. In contrast, the RKKY interaction makes the impurity spins interacting with each other via conduction electrons and thus tends to stabilize the magnetic ordering. This can be shown by the finite hybridization along with the local magnetic order at U/t (Fig. 3). Effective hybridization decreases monotonically both at impurity sites and site next to the impurity such that $\Delta_I < \Delta_{A/B}$ for all U/t consistent with the magnetic order at corresponding site. Effective hybridization at the second neighbor site decreases initially and then increases further, congruous with magnetic order.

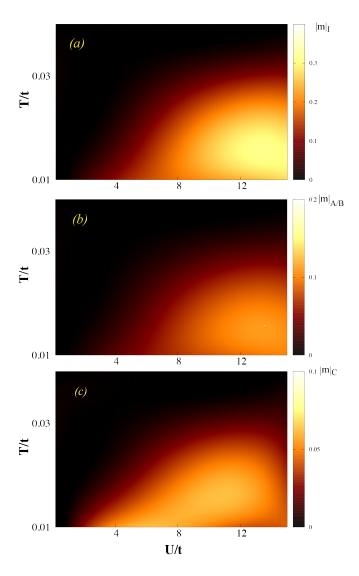


FIG. 4. Temperature vs interaction strength phase diagram of the inhomogeneous Hubbard model showing local magnetization at (a) impurity site, $m_{\rm I}$, (b) at site next to the impurity, $m_{\rm A/B}$ and (c) second neighbor site to the impurity site, $m_{\rm C}$.

B. Finite temperature calculations

We now move on to consider the effects of finite temperature in the dynamical mean-field calculations. First, it is worth to note that the current model will not show long range magnetic order due to its two-dimensional nature. Dynamical mean-field theory however does not capture long-range fluctuations, and therefore does not account for Mermin-Wagner theorem[65, 66]. Within this framework, the existence of a finite-magnetization in a DMFT calculation must be rationalized as a signature of strong magnetic correlations, as addressed in other systems[67]. In this context, while the true long range ordering temperature is at T=0, correlation lengths start to grow at a specific temperature scale $T^*>0$, and is the temperature scale captured by DMFT[67].

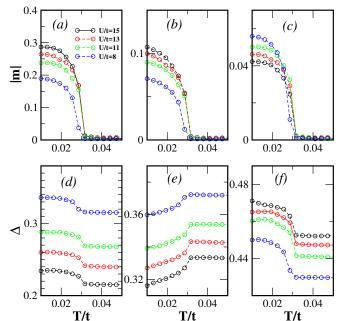


FIG. 5. Local magnetic order (a, b, c) and the corresponding effective hybridization (c, d, e) for the impurity site (a,c), site next to impurity site (b,d) and second neighbor site (c,e) of the impurity with varying temperature.

In Fig. 4, we show the region in the T-U plane where the magnetic order, m_{α} , is finite. The amplitude of m_{α} , at a given U/t, is site dependent. Local magnetization at the impurity site and at the site next to the impurity monotonically increases and then saturates with increasing interaction strength with a nonmagnetic to magnetic transition at T_c . However, the magnetic behavior at the second neighbor site gets peaked at U_p/t for a given T. U_p increases monotonically with the T. We show the spatially resolved magnetic order m_{α} the corresponding effective hybridization evaluated using CTQMC+CDMFT with varying temperature at different interaction strength U/t in the upper panels and lower panels of the Fig. 5 respectively. As the temperature is increased, the magnetic order for all the sublattices sharply disappears at T_c . The evaluation of the magnetic order at the second neighbor site is decrease with increasing value of U for a given T, opposite to the impurity site and the site next to the impurity. Effective hybridization changes with the transition temperature, with a cusp at T_c . It is important to note that the effective hybridization is finite in both magnetic and nonmagnetic regions, and the behavior of Δ is consistent with the corresponding local magnetic order.

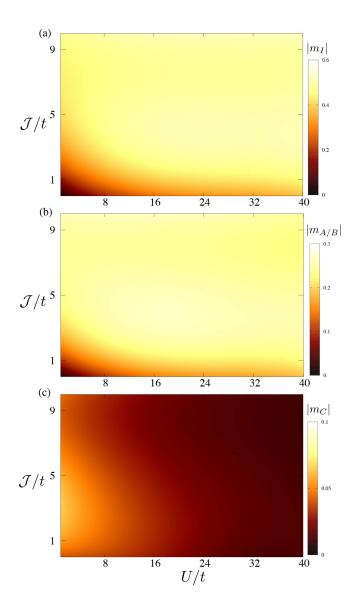


FIG. 6. Local magnetic order on (a) impurity site I, (b) flatband sites A and B, and (c) site C v.s. Hubbard U and local exchange field \mathcal{J}/t for the equivalent one dimensional model.

IV. TENSOR-NETWORK APPROACH TO THE ONE-DIMENSIONAL FLAT BAND KONDO LATTICE MODEL

We now move on to consider a one dimensional flat band Kondo lattice model, which can be rationalized as a one-dimensional version of the model outlined above. First, it is worth emphasizing that for a one-dimensional quantum many-body problem, the existence of strong quantum many-body fluctuations would prevent the system to order even in the presence of strong magnetic correlations. To accommodate this restriction, we will generalize the flat band Kondo lattice model, including local symmetry breaking terms, allowing for a selective quench of the quantum fluctuations of the system.

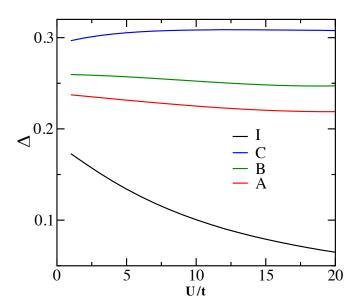


FIG. 7. Effective hybridization at different sublattice sites in the one-dimensional flat band Kondo lattice model with $\mathcal{J} = 5t$ for varying U/t.

Let us now comment on the specific model we will address. On the computational side, the interacting model can be effectively solved using tensor network methods [68–71] due to its one-dimensional nature. We will include a non-interacting hopping term in a geometry shown in Fig. 1c, and whose flat band structure is shown in Fig. 1f. Local Hubbard interactions are included in the site I as depicted in Fig. 1d. On top of the interacting term, we will also include a local exchange field on an impurity site, leading to a full Hamiltonian of the form

$$\mathcal{H} = t \sum_{\langle i,j \rangle} c_i^{\dagger} c_j + U \sum_{i \in I} \left(n_{i\uparrow} - \frac{1}{2} \right) \left(n_{i\downarrow} - \frac{1}{2} \right) + \mathcal{J} \sum_{I} S_i^z$$
(5)

Increasing the local exchange \mathcal{J} can lead to the emergence of the quasi-flat band at the site next to the impurity site, even at U=0. In a mean-field language, \mathcal{J} could be rationalized as an effective local magnetization, and therefore \mathcal{J} allows to effectively interpolate between a mean-field and purely many-body limit. In particular, when $\mathcal{J} \to \infty$, the impurity site is fully magnetized, and we are in pure mean-field limit, whereas when $\mathcal{J}=0$, the magnetic instability solely originates from U and we are in a pure many-body limit. To be concrete, we consider a chain of 40 sites (i.e., 20 lattice constants long) and compute averaged magnetization on the impurity sites I, the flat-band sites A and B, and the next the nearest site C with varying Hubbard U and the field \mathcal{J} of impurity sites. We find that the local exchange \mathcal{J} destroys quantum fluctuations and promotes a quasi-long range order at the impurity site and sites A/B. As \mathcal{J} becomes smaller, larger U is required to produce the magnetic order.

The above behavior is consistent with the hybridization effects in the two-dimensional flat band Kondo lattice addressed previously with dynamical mean-field theory. In particular, we show the effective hybridization varying with U at fixed field $\mathcal{J}=5t$ in Fig.7. We find that the effective hybridization at all sublattice sites has the same behavior as in the 2D case in Fig.3. Due to the finite exchange field \mathcal{J} , the hybridization at all sites are suppressed, with the impurity site having the largest suppression. The previous results show that, while the one-dimensional model is formally different from its two-dimensional counterpart, magnetic correlations between Kondo sites and flat band sites show a similar phenomenology.

V. CONCLUSION

Kondo lattice problems represent one of the paradigmatic many-body problems, hosting a variety of intricate phenomena due to the competitions of Kondo screening and magnetic ordering. Here, we have addressed the physics of a Kondo lattice problem, in which a conventional dispersive electron gas is replaced by a flat band electronic state. In particular, we considered flat band Kondo lattice models in both two and one dimensions, which we solved using many-body dynamical mean-field theory and tensor networks, respectively. We have demonstrated the emergence of a locally ordered state, showing how the formation of the Kondo cloud is overcome by the magnetic correlation between impurities. Interestingly, the underscreened phase observed in our many-body results can be captured via a conventional symmetry broken mean-field method, highlighting how the main features of the system are qualitatively reproduced. Our treatment focused purely on the halffilled case, yet doping of the Kondo lattice is expected to lead to a more complex interplay of the exchange and Kondo coupling scales, therefore leading to substantially more complex phase diagrams. Our results exemplify the fine interplay between magnetic ordering and manybody screening, putting forward flat band Kondo lattice models as a powerful platform to explore exotic emergent quantum many-body states.

Acknowledgments: We acknowledge the computational resources provided by the Aalto Science-IT project. J. L. L. acknowledges financial support from the Academy of Finland Projects No. 331342 and No. 336243, and the Jane and Aatos Erkko Foundation. We thank A. Ramires, P. Törmä, P. Liljeroth and M. Aapro for useful discussions.

- J. Ruostekoski, Optical kagome lattice for ultracold atoms with nearest neighbor interactions, Phys. Rev. Lett. 103, 080406 (2009).
- [2] V. I. Iglovikov, F. Hébert, B. Grémaud, G. G. Batrouni, and R. T. Scalettar, Superconducting transitions in flatband systems, Phys. Rev. B 90, 094506 (2014).
- [3] N. B. Kopnin, T. T. Heikkilä, and G. E. Volovik, High-temperature surface superconductivity in topological flat-band systems, Phys. Rev. B 83, 220503 (2011).
- [4] M. Tovmasyan, S. Peotta, P. Törmä, and S. D. Huber, Effective theory and emergent SU(2) symmetry in the flat bands of attractive hubbard models, Phys. Rev. B 94, 245149 (2016).
- [5] J. S. Hofmann, E. Berg, and D. Chowdhury, Superconductivity, pseudogap, and phase separation in topological flat bands, Phys. Rev. B 102, 201112 (2020).
- [6] V. Peri, Z.-D. Song, B. A. Bernevig, and S. D. Huber, Fragile topology and flat-band superconductivity in the strong-coupling regime, Phys. Rev. Lett. 126, 027002 (2021).
- [7] R. Drost, T. Ojanen, A. Harju, and P. Liljeroth, Topological states in engineered atomic lattices, Nature Physics 13, 668 (2017).
- [8] M. R. Slot, T. S. Gardenier, P. H. Jacobse, G. C. P. van Miert, S. N. Kempkes, S. J. M. Zevenhuizen, C. M. Smith, D. Vanmaekelbergh, and I. Swart, Experimental realization and characterization of an electronic lieb lattice, Nature Physics 13, 672 (2017).
- [9] M. N. Huda, S. Kezilebieke, and P. Liljeroth, Designer flat bands in quasi-one-dimensional atomic lattices, Phys. Rev. Research 2, 043426 (2020).

- [10] A. A. Khajetoorians, D. Wegner, A. F. Otte, and I. Swart, Creating designer quantum states of matter atom-by-atom, Nature Reviews Physics 1, 703 (2019).
- [11] G.-B. Jo, J. Guzman, C. K. Thomas, P. Hosur, A. Vishwanath, and D. M. Stamper-Kurn, Ultracold atoms in a tunable optical kagome lattice, Phys. Rev. Lett. 108, 045305 (2012).
- [12] S. Taie, H. Ozawa, T. Ichinose, T. Nishio, S. Nakajima, and Y. Takahashi, Coherent driving and freezing of bosonic matter wave in an optical lieb lattice, Science Advances 1, e1500854 (2015).
- [13] I. Bloch, J. Dalibard, and S. Nascimbène, Quantum simulations with ultracold quantum gases, Nature Physics 8, 267 (2012).
- [14] E. Suárez Morell, J. D. Correa, P. Vargas, M. Pacheco, and Z. Barticevic, Flat bands in slightly twisted bilayer graphene: Tight-binding calculations, Phys. Rev. B 82, 121407 (2010).
- [15] Y. Cao, V. Fatemi, S. Fang, K. Watanabe, T. Taniguchi, E. Kaxiras, and P. Jarillo-Herrero, Unconventional superconductivity in magic-angle graphene superlattices, Nature 556, 43 (2018).
- [16] E. Y. Andrei, D. K. Efetov, P. Jarillo-Herrero, A. H. MacDonald, K. F. Mak, T. Senthil, E. Tutuc, A. Yazdani, and A. F. Young, The marvels of moiré materials, Nature Reviews Materials 6, 201 (2021).
- [17] D. Leykam, A. Andreanov, and S. Flach, Artificial flat band systems: from lattice models to experiments, Advances in Physics: X 3, 1473052 (2018), https://doi.org/10.1080/23746149.2018.1473052.
- [18] N. B. Kopnin, T. T. Heikkilä, and G. E. Volovik,

- High-temperature surface superconductivity in topological flat-band systems, Phys. Rev. B 83, 220503 (2011).
- [19] T. T. Heikkilä, N. B. Kopnin, and G. E. Volovik, Flat bands in topological media, JETP Letters 94, 233 (2011).
- [20] O. Derzhko, J. Richter, and M. Maksymenko, Strongly correlated flat-band systems: The route from heisenberg spins to hubbard electrons, International Journal of Modern Physics B 29, 1530007 (2015), https://doi.org/10.1142/S0217979215300078.
- [21] S. Peotta and P. Törmä, Superfluidity in topologically nontrivial flat bands, Nature Communications 6, 8944 (2015).
- [22] K. Noda, K. Inaba, and M. Yamashita, Flat-band ferromagnetism in the multilayer lieb optical lattice, Phys. Rev. A 90, 043624 (2014).
- [23] Y. Cao, V. Fatemi, A. Demir, S. Fang, S. L. Tomarken, J. Y. Luo, J. D. Sanchez-Yamagishi, K. Watanabe, T. Taniguchi, E. Kaxiras, R. C. Ashoori, and P. Jarillo-Herrero, Correlated insulator behaviour at half-filling in magic-angle graphene superlattices, Nature 556, 80 EP (2018).
- [24] Y. Cao, V. Fatemi, S. Fang, K. Watanabe, T. Taniguchi, E. Kaxiras, and P. Jarillo-Herrero, Unconventional superconductivity in magic-angle graphene superlattices, Nature 556, 43 EP (2018).
- [25] M. Yankowitz, S. Chen, H. Polshyn, Y. Zhang, K. Watanabe, T. Taniguchi, D. Graf, A. F. Young, and C. R. Dean, Tuning superconductivity in twisted bilayer graphene, Science 363, 1059 (2019).
- [26] M.-T. Tran and T. T. Nguyen, Molecular kondo effect in flat-band lattices, Phys. Rev. B 97, 155125 (2018).
- [27] A. Ramires and J. L. Lado, Emulating heavy fermions in twisted trilayer graphene, Phys. Rev. Lett. 127, 026401 (2021).
- [28] Y. Jiang, X. Lai, K. Watanabe, T. Taniguchi, K. Haule, J. Mao, and E. Y. Andrei, Charge order and broken rotational symmetry in magic-angle twisted bilayer graphene, Nature 573, 91 (2019).
- [29] X. Y. Xu, K. T. Law, and P. A. Lee, Kekulé valence bond order in an extended hubbard model on the honeycomb lattice with possible applications to twisted bilayer graphene, Phys. Rev. B 98, 121406 (2018).
- [30] P. Kumar, T. I. Vanhala, and P. Törmä, Magnetization, d-wave superconductivity, and non-Fermi-liquid behavior in a crossover from dispersive to flat bands, Phys. Rev. B 100, 125141 (2019).
- [31] P. Kumar, S. Peotta, Y. Takasu, Y. Takahashi, and P. Törmä, Flat-band-induced non-fermi-liquid behavior of multicomponent fermions, Phys. Rev. A 103, L031301 (2021).
- [32] P. Coleman, New approach to the mixed-valence problem, Phys. Rev. B 29, 3035 (1984).
- [33] G. R. Stewart, Non-fermi-liquid behavior in *d* and *f*-electron metals, Rev. Mod. Phys. **73**, 797 (2001).
- [34] S. Wirth and F. Steglich, Exploring heavy fermions from macroscopic to microscopic length scales, Nature Reviews Materials 1, 10.1038/natreymats.2016.51 (2016).
- [35] H. Tsunetsugu, M. Sigrist, and K. Ueda, The groundstate phase diagram of the one-dimensional kondo lattice model, Rev. Mod. Phys. 69, 809 (1997).
- [36] Q. Si and F. Steglich, Heavy fermions and quantum phase transitions, Science 329, 1161 (2010).
- [37] P. Coleman, Heavy fermions and the kondo lattice: a 21st century perspective, arXiv preprint arXiv:1509.05769

- (2015).
- [38] A. Ramires and P. Coleman, Theory of the electron spin resonance in the heavy fermion metal β -ybalb₄, Phys. Rev. Lett. **112**, 116405 (2014).
- [39] A. Ramires and P. Coleman, Supersymmetric approach to heavy fermion systems, Phys. Rev. B 93, 035120 (2016).
- [40] V. Vaňo, M. Amini, S. C. Ganguli, G. Chen, J. L. Lado, S. Kezilebieke, and P. Liljeroth, Artificial heavy fermions in a van der Waals heterostructure, arXiv e-prints, arXiv:2103.11989 (2021), arXiv:2103.11989 [cond-mat.mes-hall].
- [41] M. Dzero, K. Sun, V. Galitski, and P. Coleman, Topological kondo insulators, Phys. Rev. Lett. 104, 106408 (2010).
- [42] M. Dzero, J. Xia, V. Galitski, and P. Coleman, Topological kondo insulators, Annual Review of Condensed Matter Physics 7, 249 (2016).
- [43] M. Legner, A. Rüegg, and M. Sigrist, Surface-state spin textures and mirror chern numbers in topological kondo insulators, Phys. Rev. Lett. 115, 156405 (2015).
- [44] L. Jiao, S. Howard, S. Ran, Z. Wang, J. O. Rodriguez, M. Sigrist, Z. Wang, N. P. Butch, and V. Madhavan, Chiral superconductivity in heavy-fermion metal UTe2, Nature 579, 523 (2020).
- [45] I. Titvinidze, A. Schwabe, and M. Potthoff, Ferromagnetism of magnetic impurities coupled indirectly via conduction electrons: Insights from various theoretical approaches, Phys. Rev. B 90, 045112 (2014).
- [46] A. Schwabe, I. Titvinidze, and M. Potthoff, Inverse indirect magnetic exchange, Phys. Rev. B 88, 121107 (2013).
- [47] N. C. Costa, M. V. Araújo, J. P. Lima, T. Paiva, R. R. dos Santos, and R. T. Scalettar, Compressible ferrimagnetism in the depleted periodic anderson model, Phys. Rev. B 97, 085123 (2018).
- [48] A. Ramires and J. L. Lado, Impurity-induced triple point fermions in twisted bilayer graphene, Phys. Rev. B 99, 245118 (2019).
- [49] A. Lopez-Bezanilla and J. L. Lado, Defect-induced magnetism and yu-shiba-rusinov states in twisted bilayer graphene, Phys. Rev. Materials 3, 084003 (2019).
- [50] M. A. Ruderman and C. Kittel, Indirect exchange coupling of nuclear magnetic moments by conduction electrons, Phys. Rev. 96, 99 (1954).
- [51] K. Yosida, Magnetic properties of cu-mn alloys, Phys. Rev. 106, 893 (1957).
- [52] T. Kasuya, A theory of metallic ferro- and antiferromagnetism on zener's model, Progress of Theoretical Physics 16, 45 (1956).
- [53] B. Sutherland, Localization of electronic wave functions due to local topology, Phys. Rev. B 34, 5208 (1986).
- [54] P. W. Brouwer, E. Racine, A. Furusaki, Y. Hatsugai, Y. Morita, and C. Mudry, Zero modes in the random hopping model, Phys. Rev. B 66, 014204 (2002).
- [55] A. Mielke, Ferromagnetism in the hubbard model on line graphs and further considerations, Journal of Physics A: Mathematical and General 24, 3311 (1991).
- [56] E. H. Lieb, Two theorems on the hubbard model, Phys. Rev. Lett. 62, 1201 (1989).
- [57] A. Georges, G. Kotliar, W. Krauth, and M. J. Rozenberg, Dynamical mean-field theory of strongly correlated fermion systems and the limit of infinite dimensions, Rev. Mod. Phys. 68, 13 (1996).
- [58] F. F. Assaad and T. C. Lang, Diagrammatic determinan-

- tal quantum monte carlo methods: Projective schemes and applications to the hubbard-holstein model, Phys. Rev. B **76**, 035116 (2007).
- [59] E. Gull, Continuous-Time Quantum Montecarlo Algorithms for Fermions, Ph.D. thesis, ETH ZURICH (2008).
- [60] T. I. Vanhala and P. Törmä, Dynamical mean-field theory study of stripe order and d-wave superconductivity in the two-dimensional hubbard model, Phys. Rev. B 97, 075112 (2018).
- [61] A. I. Lichtenstein and M. I. Katsnelson, Antiferromagnetism and d-wave superconductivity in cuprates: A cluster dynamical mean-field theory, Phys. Rev. B 62, R9283 (2000).
- [62] M. Capone and G. Kotliar, Competition between d-wave superconductivity and antiferromagnetism in the twodimensional hubbard model, Phys. Rev. B 74, 054513 (2006).
- [63] S. Burdin and P. Fulde, Random kondo alloys investigated with the coherent potential approximation, Phys. Rev. B 76, 104425 (2007).

- [64] J. E. Hirsch, Two-dimensional hubbard model: Numerical simulation study, Phys. Rev. B 31, 4403 (1985).
- [65] N. D. Mermin and H. Wagner, Absence of ferromagnetism or antiferromagnetism in one- or two-dimensional isotropic heisenberg models, Phys. Rev. Lett. 17, 1133 (1966).
- [66] P. C. Hohenberg, Existence of long-range order in one and two dimensions, Phys. Rev. 158, 383 (1967).
- [67] L. Fratino, P. Sémon, M. Charlebois, G. Sordi, and A.-M. S. Tremblay, Signatures of the mott transition in the antiferromagnetic state of the two-dimensional hubbard model, Phys. Rev. B 95, 235109 (2017).
- [68] S. R. White, Density matrix formulation for quantum renormalization groups, Phys. Rev. Lett. 69, 2863 (1992).
- [69] M. Fishman, S. R. White, and E. M. Stoudenmire, The ITensor Software Library for Tensor Network Calculations, arXiv:2007.14822 [cs.MS].
- [70] ITensor Library http://itensor.org.
- [71] DMRGpy Library https://github.com/joselado/dmrgpy.